ISSN 1674-1056
http://cpb.iphy.ac.cn
http://iopscience.iop.org/cpb
中国物理 B
Chinese Physics
中国物理 Chinese Physics B

Nanoforest-like CdS/TiO_2 heterostructure composites: Synthesis and photoelectrochemical application

Shi Su(苏适), Jinwen Ma(马晋文), Wanlong Zuo(左万龙), Jun Wang(汪俊), Li Liu(刘莉), Shuang Feng(冯爽), Tie Liu(刘铁), Wuyou Fu(付乌有), Haibin Yang(杨海滨)

Citation: Chin. Phys. B . 2018, 27(8): 088802. **doi:** 10.1088/1674-1056/27/8/088802

Journal homepage: http://cpb.iphy.ac.cn; http://iopscience.iop.org/cpb

What follows is a list of articles you may be interested in

Precisely tuning Ge substitution for efficient solution-processed $Cu_2ZnSn(S, Se)_4$ solar cells

Xinshou Wang(王新收), Dongxing Kou(寇东星), Wenhui Zhou(周文辉), Zhengji Zhou(周正基), Qingwen Tian(田庆文), Yuena Meng(孟月娜), Sixin Wu(武四新)

Chin. Phys. B . 2018, 27(1): 018809. **doi:** 10.1088/1674-1056/27/1/018809

Performance improvement of $CdS/Cu(In,Ga)Se_2$ solar cells after rapid thermal annealing

Chen Dong-Sheng, Yang Jie, Xu Fei, Zhou Ping-Hua, Du Hui-Wei, Shi Jian-Wei, Yu Zheng-Shan, Zhang Yu-Hong, Brian Bartholomeusz, Ma Zhong-Quan

Chin. Phys. B . 2013, 22(1): 018801. **doi:** 10.1088/1674-1056/22/1/018801

Nanoforest-like CdS/TiO_2 heterostructure composites: Synthesis and photoelectrochemical application*

Shi Su(苏适)[1], Jinwen Ma(马晋文)[2], Wanlong Zuo(左万龙)[3], Jun Wang(汪俊)[1], Li Liu(刘莉)[1], Shuang Feng(冯爽)[1], Tie Liu(刘铁)[1], Wuyou Fu(付乌有)[1], and Haibin Yang(杨海滨)[1,†]

[1] *State Key Laboratory of Superhard Materials, Jilin University, Changchun* 130012, *China*
[2] *College of New Energy, Bohai University, Jinzhou* 121013, *China*
[3] *Anhui Provincial Key Laboratory of Optoelectric Materials Science and Technology, Anhui Normal University, Wuhu* 241000, *China*

(Received 22 March 2018; revised manuscript received 22 May 2018; published online 25 July 2018)

In this study, TiO_2 nanoforest films consisting of nanotubes have been synthesized by a simple hydrothermal method and a subsequent sintering technique. The hydrothermal reaction time is important for the controlling of the nanotube diameter and the specific surface area of holistic TiO_2 films. When the hydrothermal process reaction time is up to 8 hours, the diameter of the nanotube is about 10 nm, and the specific surface area of TiO_2 nanoforest films reaches the maximum. CdS nanoparticles are synthesized on TiO_2 nanoforest films by the successive ionic layer adsorption and reaction (SILAR) technique. The transmission electron microscope (TEM) and energy dispersive x-ray spectroscopy (EDX) mapping results verify that TiO_2/CdS heterostructures are realized. A significant red-shift of the absorption edge from 380 nm to 540 nm can be observed after the pure TiO_2 film is sensitized by CdS nanoparticles. Under irradiation of light, the current density of the optimal TiO_2/CdS photoanode is 2.30 mA·cm^{-2} at 0 V relative to the saturated calomel electrode (SCE), which is 6 times stronger than that of the pure TiO_2 photoanode. This study suggests that the TiO_2 nanoforest consisting of interlinked pony-size nanotubes is a promising nanostructure for photoelectrochemical.

Keywords: TiO_2, nanoforest, CdS, photoelectrochemical

PACS: 88.30.mj, 88.40.ff **DOI:** 10.1088/1674-1056/27/8/088802

1. Introduction

Photoelectrochemical (PEC) cell is an important way of solar–to–electric energy conversion.[1] The traditional PEC cell is comprised of a photoanode and a counter electrode in electrolyte solution. In order to improve the photoelectric conversion efficiency, photoanode materials should have excellent photoresponse, separation of charge, and electrons transference.[2–4] TiO_2 is a widely used material in the photoanode of PEC cells, due to its merits of proper electronic band structure, fine chemical stability, and good photocorrosion resistance.[5–7] In particular, TiO_2 nanorods or nanotubes, as a typical one-dimensional material, can provide a direct conduction pathway for the photogenerated electrons, and less grain boundary compared to TiO_2 nanoparticles framework results in reduced recombination opportunity of photogenerated carriers.[8–10] However, TiO_2 can only absorb electromagnetic waves of the ultraviolet band due to its large band gap (3.2 eV), resulting in a low photovoltaic conversion efficiency.[10] To broaden the photoresponse range of sole TiO_2, one frequently used way is to sensitize TiO_2 with small gap semiconductors, such as Bi_2S_3, PbS, CdS, and CdSe, which are defined as quantum dot sensitization solar cells (QDSCs).[11–20]

There are several notable points about quantum dots (QDs) that would affect their PEC performance: QDs species, dispersity, quantity, and so on, which can be controlled by QDs species selection and growth technology. For QDs species selection, the position of conduction band (CB) edge is a key point. When the CB of TiO_2 is lower than that of small band gap semiconductor, the photogenerated electrons will be injected to the CB of TiO_2 from the small band gap semiconductor due to the electric field driving force of heterojunction.[21,22] CdS is a narrow gap semiconductor ($E_g = 2.42$ eV), and its CB is more negative than that of TiO_2. Thus, based on the aforementioned factors, CdS is a promising sensitizer for TiO_2 nanostructure.[11,17] It is a type II structure between TiO_2 and CdS, as shown in Fig. 1.[11,16,17] For QDs growth technology, numerous methods have been reported, such as single-step electrodeposition, electrochemical atomic layer deposition, and successive ionic layer adsorption and reaction method (SILAR).[23–25] Among them, SILAR is an outstanding way to obtain QDs. In a typical SILAR process, anion and cation will first be adsorbed on the surface dangling bond of TiO_2, then nucleate when the concentration is saturated and grow up as the SILAR cycles increases.[23] It is worth emphasizing that the correlation between ions and TiO_2 is chemical adsorption rather than physisorption, from which we obtained a large number of efficient heterojunction regions. Furthermore, in order to further expand the heterojunction re-

*Project supported by the National Natural Science Foundation of China (Grant Nos. 51272086 and 11704004), the Technology Development Program of Jilin Province, China (Grant No. 20130206078GX), and the Natural Science Foundation of Anhui Province, China (Grant No. 1808085QA20).

†Corresponding author. E-mail: yanghb@jlu.edu.cn

© 2018 Chinese Physical Society and IOP Publishing Ltd

gion area, the TiO_2 nanostructure with high surface area and higher activity is needed. In morphology, the smaller the size of the material is, the larger the surface area can be obtained. As reported, Kim and his co-worker prepared a tangled TiO_2 forest which showed extreme superhydrophobic performance due to its large surface area.[26] However, as far as we know, the PEC performance of similar mini size TiO_2 nanotube has been rarely studied.

In the recent work, we have synthesized TiO_2 nanoforest films which consist of about 10-nm diameter nanotubes by a simple solvothermal method on Ti foils. We obtain a large amount of surface area of heterojunctions due to the small diameter and the large length of TiO_2. As a result, 10-nm TiO_2 nanoforest can load much more QDs. The PEC properties and optical properties of CdS QDs sensitized TiO_2 nanoforest photoanodes have been thoroughly studied. The results clearly demonstrate that a large surface area is necessary for excellent PEC performance, and the TiO_2 nanoforest consisting of 10-nm diameter nanotubes is a promising PEC and photocatalysis material.

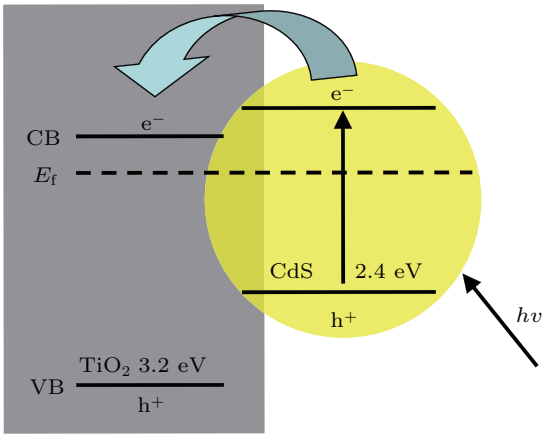


Fig. 1. (color online) Energy band structure of CdS QDs sensitized TiO_2 nanoforest.

2. Experiments

2.1. Synthesis of TiO_2 nanoforest films

The TiO_2 nanoforest films were obtained by a combining method of hydrothermal process and a subsequent sintering technique, according to Kim's report.[26] Firstly, a cleaned Ti foil (99.9% purity) was immersed into a Teflon-lined autoclave which contained 10-M NaOH aqueous solution, and heated in an electric oven at 140 °C for several hours. When autoclave was cooled to room temperature, the Ti foil was taken out and rinsed with flowing deionized water, then immersed into 0.1-M HCl aqueous solution for 3 min, and rinsed with flowing deionized water again. After drying in an oven at 80 °C, the samples were annealed at 450 °C for 3 h in air. The prepared TiO_2 films with different hydrothermal reaction times were designated as TiO_2(x h) ($x = 2, 4, 6, 8$) hereinafter.

2.2. Preparation of CdS QDs sensitized TiO_2 nanoforest films

CdS QDs sensitizing process has been reported in our previous work.[27] In a typical process, the TiO_2 films were sequentially immersed into ethanol solution of $Cd(NO_3)_2{\cdot}4H_2O$, the $Na_2S{\cdot}9H_2O$ mixed solution of methanol, and deionized water for 5 min each. Following each immersion, rinsing process with pure ethanol and deionized water and drying process were necessary in order to remove excess precursors. This is one SILAR cycle. The amount of CdS QDs can be adjusted by altering the number of SILAR cycles. The achieved composite films with different CdS SILAR cycles were designated as TiO_2(x h)/CdS(y c) ($y = 1$–7) hereinafter.

2.3. Characterization

The field emission scanning electron microscopy (FE-SEM, JEOL JSM–6700F, 8 kV) was performed to characterize the morphology and the size. The transmission electron microscope (TEM, JEM–2100F, 200 kV) was used to determine the crystallographic directions. The high angle annular dark field STEM (HAADF STEM) image and the corresponding energy dispersive x-ray spectroscopy (EDX) investigations were carried out by an FEI Magellan 400 microscope. X-ray power diffraction (XRD) analysis was conducted on an x-ray diffractometer (Rigaku D/max–2500) with Cu K_α radiation ($\lambda = 1.5418$ Å). UV-visible absorption was performed using a UV–3150 double–beam spectrophotometer.

2.4. Photoelectrochemical measurements

Three-electrode electrochemistry system was adopted to test PEC properties with the prepared samples as photoanode electrode. A platinum mesh was used as the counter electrode and a saturated calomel electrode (SCE) was used as the reference electrode. The electrolyte was a mixture of 0.25-M Na_2S and 0.35-M Na_2SO_3 aqueous solution. A 500-W xenon lamp was used to simulate sunlight. The light intensity was calibrated to 100 mW·cm^{-2} by a laser power meter. The active area was 1 cm^2. In addition, for better comparison with the photocurrent density of other works, the potentials of the working electrodes can be calculated using the formula $V(\text{RHE}) = V(\text{SCE}) + 0.0591 * \text{pH} + 0.244$ V, where V(RHE) is a potential relative to the reversible hydrogen potential, V(SCE) is a potential relative to the SCE electrode, and pH = 13.2 is the pH value of the electrolyte.

3. Results and discussion

3.1. Characterization of TiO_2 nanoforest films

3.1.1. Morphologies of TiO_2 nanoforest films

Figures 2(a)–2(d) show the top view FESEM images of the obtained TiO_2 nanoforest films with different hydrother-

mal reaction times (2 h, 4 h, 6 h, and 8 h). When the hydrothermal reaction time is 2 h, as shown in Fig. 2(a), the surface of the Ti foil is etched to form multiple ribbon-shaped nanostructures with an average diameter of 100 nm which share a head. The hydrothermal reaction time is so short that the etching process of Ti foil is not sufficient, resulting in the exposure of a large area of Ti foil. As the hydrothermal reaction time extends, almost the entire Ti foil is etched, and the previous ribbon-shaped nanostructures are transformed into many gracile nanotubes. The nanotubes associate with each other, forme a nanotube network at first (Fig. 2(b)), and finally evolve into nanoforest (Figs. 2(c) and 2(d)). Simultaneously, the length of nanotubes increase gradually, as shown in Figs. 2(b)–2(d). In particular, when the hydrothermal reaction time is 8 h (Fig. 2(d)), the length of the nanotube increase to several micrometers. Figure 2(e) shows a cross-sectional view FESEM image of the TiO_2(8 h) film. Most of the nanotubes grow perpendicularly to the Ti foil substrate, just like a trunk. The top TiO_2 nanotubes are curved and overlap with each other, just like dense branches grow leaves. In addition, this image displays that the thickness of the TiO_2 nanoforest is about 3 μm. The TEM micrograph shown in Fig. 2(f) reveals that the long nanostructure is indeed nanotube with an average diameter about 10 nm. In summary, we can draw the conclusion that the surface area of the obtained TiO_2 nanoforest increases with time. In addition, a 10-h hydrothermal experiment has been conducted. However, the obtained TiO_2 thin film easily falls out from the Ti foil, which is significantly different from the good adhesion of other TiO_2 nanotubes on the Ti substrate (2 h–8 h). This may be attributed to the fact that the obtained TiO_2 nanotubes are too long to be fastened to the Ti substrate. Therefore, we determine the time limit is 8 h in our experiment.

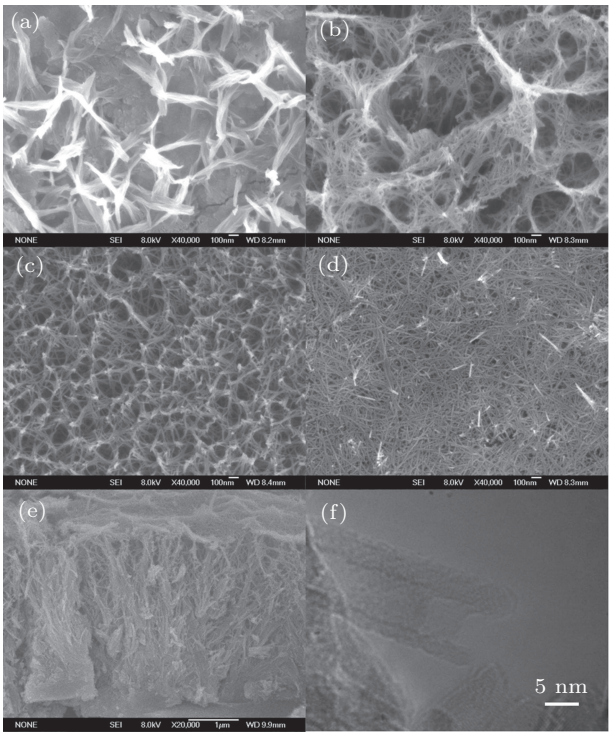


Fig. 2. (a)–(d) Top view FESEM images of TiO_2 nanoforest films with different hydrothermal reaction times (2 h, 4 h, 6 h, and 8 h, respectively); (e) cross–sectional view FESEM image of TiO_2(8 h); (f) TEM image of TiO_2(8 h).

3.1.2. Crystalline phase structure of TiO_2 nanoforest films

Figure 3 displays the XRD patterns of the TiO_2 nanoforest films with different hydrothermal reaction times. For TiO_2(4 h), there are two peaks at 21.21° and 26.35° which can be indexed to $Na_2Ti_6O_{13}$ and Ti_4O_7, respectively. Both peaks disappear for TiO_2(6 h) and TiO_2(8 h). For all the samples, the diffraction peaks at 25.40° and 48.16° can be indexed to the (101) and (200) lattice planes of anatase TiO_2 (JCPDS no. 73–1764). The rest of the diffraction peaks in the XRD patterns can be indexed to the hexagonal Ti (JCPDS no. 44–1294). Moreover, the (101) and (200) diffraction peaks of anatase structure of TiO_2 increase gradually with the increase of the hydrothermal reaction time, with TiO_2(8 h) being exceptionally intensified, which indicates that the crystallization properties of TiO_2 nanoforest films are getting better as the hydrothermal reaction time increases, and the best one is TiO_2(8 h).

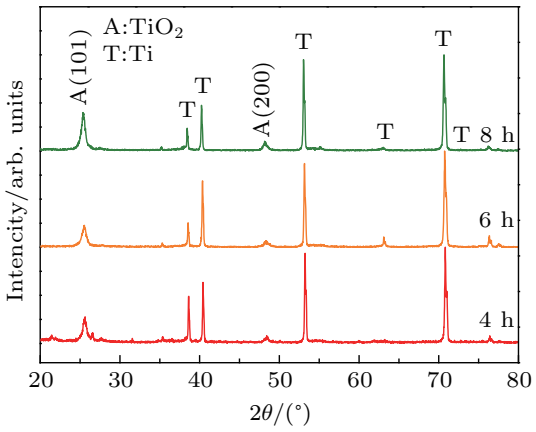


Fig. 3. (color online) XRD patterns of TiO_2 nanoforest films with different hydrothermal reaction times (4 h–8 h).

3.1.3. Photoelectrochemical performance of TiO_2 nanoforest films

Figure 4 shows characteristic J–V curves of the TiO_2(x h) (x = 4 h–8 h) nanoforest films at different times. All the TiO_2 nanoforest films show a negligible photocurrent density under the dark condition. In the case of light illumination, the photocurrent density of TiO_2 nanoforest films increases rapidly with the increase of the hydrothermal reaction time. TiO_2(8 h) shows an optimal photocurrent density of 0.38 mA·cm^{-2} at 0 V, which is 2.4 times larger than 0.16 mA·cm^{-2} of TiO_2(4 h). It can be ascribed to its denser nanotube and larger surface

area. The formation of the nanotube forest makes a much larger solid–liquid boundary area between the photoelectrodes and the electrolyte, which is beneficial to accelerate the separation of photogenerated electrons and holes, thereby optimizing the PEC performance of the TiO_2 photoanode.

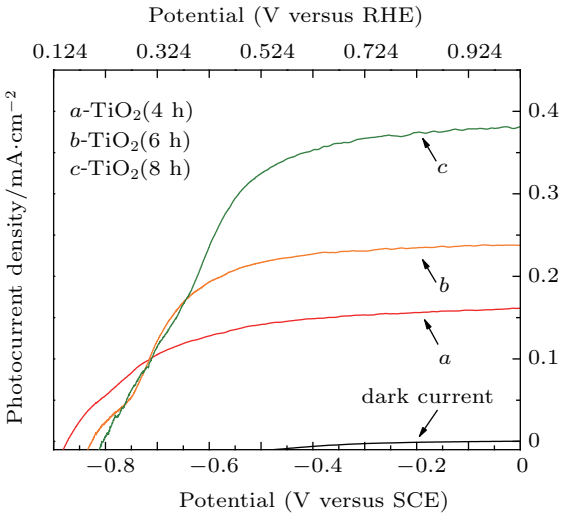


Fig. 4. (color online) Characteristic J–V curves of the $TiO_2(x$ h) ($x = 4$ h–8 h) nanoforest films at different times.

3.2. Characterization of CdS sensitized TiO_2 nanoforest films

3.2.1. Morphologies of CdS sensitized TiO_2 nanoforest films

Figure 5(a) shows a typical FESEM image of CdS sensitized TiO_2 nanoforest film (TiO_2(8 h)/CdS(5 c)). Obviously, the surface of TiO_2 nanotubes becomes rough after CdS sensitization, and the distribution of CdS nanoparticles on TiO_2 nanotubes is fairly uniform. We attribute the successful growth of CdS QDs to the surface electronegativity of TiO_2 nanotubes.[23,28] Figure 5(b) shows the HAADF STEM image of TiO_2(8 h)/CdS(5 c). It clearly indicates that the long TiO_2 nanostructures are nanotubes. In addition, according to the test principle of HAADF STEM, we can identify the bright spots on nanotubes are CdS QDs, which further confirms that CdS QDs with a diameter of about 5 nm–10 nm are distributed on the nanotubes homogeneously.

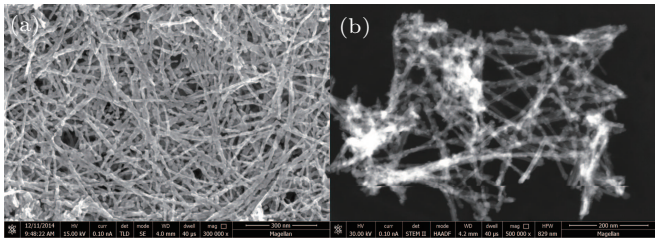


Fig. 5. (a) The FESEM and (b) HAADF STEM image of CdS sensitized TiO_2 nanoforest film (TiO_2(8 h)/CdS(5 c)).

3.2.2. Phase composition and crystalline structure of CdS sensitized TiO_2 nanoforest films

Figure 6(a) shows the XRD pattern of the prepared TiO_2(8 h)/CdS(5 c) film. As compared to the bare TiO_2(8 h) film (Fig. 2(d)), TiO_2(8 h)/CdS(5 c) film exhibit several new diffraction peaks at 2θ of ca. 26.44°, 30.64° and 43.92°, corresponding to the {111}, {200}, and {220} planes of cubic-phase CdS [JCPDS no. 65–2887], respectively. To further visually determine the distribution of CdS QDs, we have performed STEM EDX mapping analysis of TiO_2(8 h)/CdS(5 c), which corresponds to the TEM image of Fig. 5(b). Figure 6(b) is the STEM EDX mapping of both Ti and Cd elements, which represent the compound of TiO_2 and CdS, respectively. It clearly shows that the distribution of Ti element is continuous while discrete for Cd element, which reveals that CdS QDs are interspersed on TiO_2 nanotubes. Figures 6(c)–6(f) are the STEM EDX mapping of O, Ti, S, and Cd elements in sequence, which reveals that the distributions of all the elements are completely consistent with the TiO_2 nanotube arrangement. In addition, by comparing Figs. 6(e) and 6(f), it is found that the existing Cd element appears to be more than the S element; this can be attributed to the fact that the surface of TiO_2 is negatively charged, and it is physically easy to combine with a cation, Cd^{2+}. All the results conclusively confirm the chemical composition that CdS QDs have grown on the TiO_2 nanotubes and distributed homogeneously.

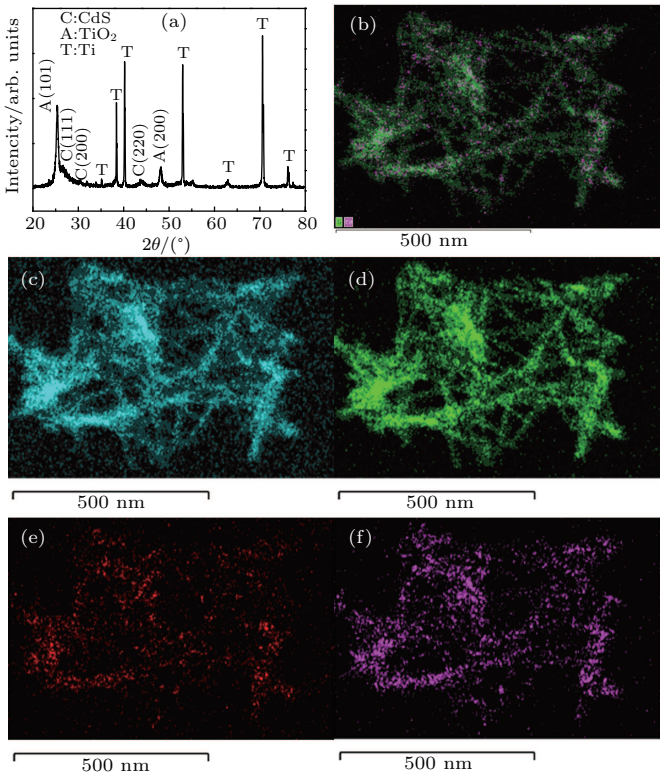


Fig. 6. (color online) (a) XRD pattern of TiO_2(8 h)/CdS(5 c) film. STEM EDX mapping of (b) Ti & Cd elements, (c)–(f) O, Ti, S, and Cd elements of TiO_2(8 h)/CdS(5 c) film.

3.2.3. UV–visible absorption spectroscopy of CdS sensitized TiO_2 nanoforest films

In order to verify the effect of CdS on the photoresponse range, UV–visible diffuse reflectance tests of various CdS sensitized TiO_2 photoanodes were conducted. The

corresponding transformed absorption spectra are shown in Figs. 7(a) and 7(b). Figure 7(a) shows the absorption spectra of TiO_2(8 h)/CdS with different CdS SILAR cycles. The absorption edge of TiO_2(8 h) film is $\sim$ 380 nm, with no absorption in the visible region. In contrast, the spectra of electrodes after CdS sensitization show obvious absorption in the visible region, and all the absorption edges follow the red shift law as the CdS deposition cycles increases. Finally, TiO_2(8 h)/CdS(7 c) shows the broadest absorption range with an absorption edge of up to $\sim$ 540 nm. These variations indicate that CdS is an appropriate sensitizer for TiO_2 photoanode to extend its photoresponse region. The red-shift of the absorption edge indicates that the CdS particle is growing, and its band gap is decreasing, corresponding to the quantum confinement effect.[29,30]

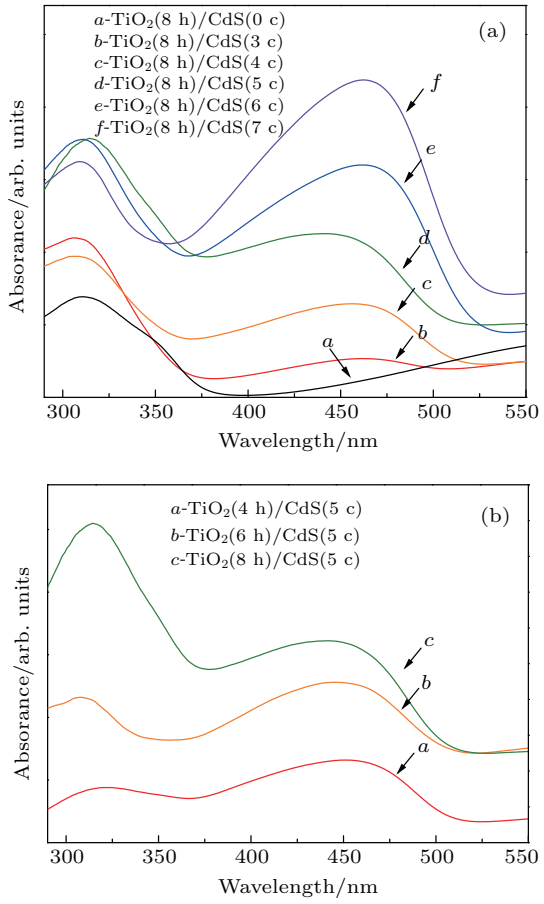


Fig. 7. (color online) UV–Vis diffuse reflectance spectrum of (a) TiO_2(8 h)/CdS(y c) (y = 0, 3–7) and (b) TiO_2(x h)/CdS(5 c) (x = 4–8).

Moreover, in order to understand the influence of different hydrothermal reaction times on the sensitized effect, we also conducted the UV–visible absorption investigation of TiO_2(x h)/CdS(5 c) (x = 4–8), as shown in Fig. 7(b). It clearly reveals that the visible light absorptivity of TiO_2(x h)/CdS increases with the hydrothermal reaction time of TiO_2. This is mainly attributed to the fact that the surface area of TiO_2 nanoforest films increases with the hydrothermal reaction time, as shown in Figs. 2(a)–2(d). As we know, increased surface area can provide more sensitizer loading area, subsequently leading to stronger light harvesting. Based on the UV–visible absorption spectroscopy, we deduce that the optimal hydrothermal reaction time for TiO_2 nanoforest film is 8 h in this experimental study.

3.2.4. Photoelectrochemical performance of the CdS sensitized TiO_2 nanoforest films

Figure 8(a) shows the J–V curves of TiO_2(8 h) and TiO_2(8 h)/CdS(y c) (y = 3–7). Dark current can be ignored for all samples. We mainly discuss the current density variation at 0 V relative to SCE and the onset potential variation under light illumination. Apparently, the photocurrent density of TiO_2(8 h) is very small, just 0.38 mA·cm^{-2}. However, the photocurrent density of TiO_2(8 h)/CdS photoanodes shows a great improvement, and increases with the increase of CdS SILAR cycles to a certain extent. When the SILAR sensitization cycles is 5, the photocurrent density reaches the maximum of 2.30 mA·cm^{-2}, which is about 6 times of that of the pristine TiO_2(8 h). After that, if the number of SILAR cycles continues to increase, the current will be reduced. For example, the photocurrent density of TiO_2(8 h)/CdS(6 c) is 1.98 mA·cm^{-2}. We sum up the reasons of the above as follows. Firstly, CdS QDs broaden the visible light absorption range of the electrode, and then increase the concentration of the photogenerated carriers. Secondly, a typical type-II structure has been formed between TiO_2 and CdS, which is beneficial to the charge separation.[31] Thirdly, the size and the quantity of CdS grains increase with the increase of the SILAR cycles. When they rise to a certain extent, the dominance of QD will be lost, and the recombination traps will increase, resulting in the deterioration of PEC performance.[32,33] Besides, the onset potential of electrodes increases after the CdS sensitization. The onset potential value of the plain TiO_2(8 h) photoanode is 0.80 V, while it is about 1.03 V–1.09 V for the TiO_2(8 h)/CdS(y c) photoanodes. According to the definition of the voltage generated under illumination, the varying onset potentials signify that a heterojunction is generated between the interface of TiO_2 and CdS, and that the E_f alignment occurs between TiO_2 and CdS.[2,34]

Figure 8(b) shows the comparison of J–V curves for TiO_2(x h)/CdS(5 c) (x = 4–8). It clearly reveals that the photocurrent density of TiO_2(xh)/CdS(5 c) increases with the hydrothermal reaction time of TiO_2, and the TiO_2(8 h)/CdS(5 c) photoanode exhibits the best PEC performance, showing the same regularity as the UV–visible absorption spectrum (Fig. 7(b)). This can be summed up in a few steps. Firstly, the surface area of TiO_2 nanoforest films increases as the hydrothermal reaction time extends. Secondly, increased surface areas can provide more sensitizer loading area, subsequently leading to stronger optical harvesting when the CdS deposition cycle is kept at a constant value. Thirdly, the enhanced

optical absorption helps to boost the amount of electron–hole pairs, providing a great quantity of carriers. Fourthly, a larger amount of CdS means larger heterostructure areas of TiO_2/CdS, which creates a more efficient charge transfer channel, and thus facilitates electron transport from CdS to TiO_2 in the type-II stepwise band-edge.

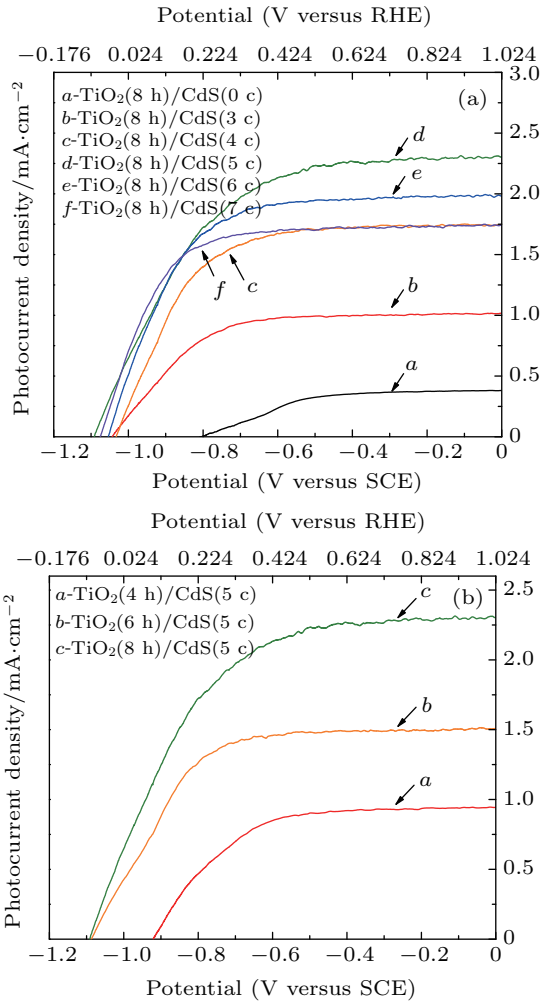


Fig. 8. (color online) Characteristic *J*–*V* curves of (a) TiO_2(8 h)/CdS(*y* c) (*y* = 0, 3–7) and (b) TiO_2(*x* h)/CdS(5 c) (*x* = 4–8).

4. Conclusions

In summary, CdS QDs sensitized TiO_2 nanoforest films are obtained and studied in this report. TiO_2 nanoforest films consisting of nanotubes have been synthesized on Ti foils by a hydrothermal process and a subsequent sintering technique. The obtained TiO_2 nanoforest films with different growth times are characterized in detail by XRD, SEM, and *J*–*V* curves. The data suggested that the hydrothermal reaction time has a direct impact on the structure, morphology, and PEC performance of TiO_2 nanoforest film. CdS nanoparticles are deposited on TiO_2 nanoforest films by SILAR technique. TiO_2/CdS heterostructures broaden the photoresponse range from the ultraviolet region to the visible region, and improve the photoelectrochemical performance significantly. This obvious improvement can be attributed to two main reasons. Firstly, the TiO_2 nanoforest films provide a large surface area for the attached CdS QDs, which leads to a large photogenerated carrier yield Secondly, the interlinked 1D TiO_2 nanotubes provide direct pathways for photogenerated charge. This study suggests that the TiO_2 nanoforest consisting of interlinked nanotubes is a promising nanostructure for PEC and photocatalysis application.

References

[1] Grätzel M 2001 *Nature* **414** 338
[2] O'Regan B and Grätzel M 1991 *Nature* **353** 737
[3] Li Z, Luo W, Zhang M, Feng J and Zou Z 2013 *Energy Environ. Sci.* **6** 347
[4] Xu J, Hu Z, Zhang J, Xiong W, Sun L, Wan L, Zhou R, Jiang Y and Lee C 2017 *J. Mater. Chem. A* **5** 25230
[5] Choi H, Sofranko A C and Dionysiou D D 2006 *Adv. Funct. Mater.* **16** 1067
[6] Shahzad N, Risplendi F, Pugliese D, Bianco S, Sacco A, Lamberti A, Gazia R, Tresso E and Cicero G 2013 *J. Phys. Chem.* C **117** 22778
[7] Fu W, Li G, Wang Y, Zeng S, Yan Z, Wang J, Xin S, Zhang L, Wu S and Zhang Z 2018 *Chem. Commun.* **54** 58
[8] Li S, Qiu J, Ling M, Peng F, Wood B and Zhang S 2013 *ACS Appl. Mater. Interfaces* **5** 11129
[9] Cao F, Xiong J, Wu F, Liu Q, Shi Z, Yu Y, Wang X and Li L 2016 *ACS Appl. Mater. Interfaces* **8** 12239
[10] Shao F, Sun J, Gao L, Yang S and Luo J 2011 *J. Phys. Chem. C* **115** 1819
[11] Sun W, Yu Y, Pan H, Gao X, Chen Q and Peng L 2008 *J. Am. Chem. Soc.* **130** 1124
[12] Tian J, Zhang Q, Zhang L, Gao R, Shen L, Zhang S, Qu X and Cao G 2013 *Nanoscale* **5** 936
[13] Robel I, Kuno M and Kamat P 2007 *J. Am. Chem. Soc.* **129** 4136
[14] Etgar L, Yanover D, Čapek R K, Vaxenburg R, Xue Z, Liu B, Nazeeruddin M K, Lifshitz E and Grätzel M 2013 *Adv. Funct. Mater.* **23** 2736
[15] Li Z, Yu L, Liu Y and Sun S 2014 *J. Mater. Sci.* **49** 6392
[16] Li X, Liu H, Luo D, Li J, Huang Y, Li H, Fang Y, Xu Y and Zhu L 2012 *Chem. Eng. J.* **180** 151
[17] Pan R, Wu Y and Liew K 2010 *Appl. Surf. Sci.* **256** 6564
[18] Luo S, Shen H, Hu W, Yao Z, Li J, Oron D, Wang N and Lin H 2016 *RSC Adv.* **6** 21156
[19] Zolfaghari-Isavandi Z and Shariatinia Z 2018 *J. Alloys Compd.* **737** 99
[20] Nguyen V M, Cai Q Y and Grimes C A 2016 *J. Colloid Interf. Sci.* **483** 287
[21] Su W, Chen J, Wu L, Wang X, Wang X and Fu X 2008 *Appl. Catal. B-Environ.* **77** 264
[22] Seol M, Jang J, Cho S, Lee J S and Yong K 2013 *Chem. Mater.* **25** 184
[23] Nicolau Y F 1985 *Appl. Surf. Sci.* **22/23** 1061
[24] Banerjee S, Mohapatra S K, Das P P and Misra M 2008 *Chem. Mater.* **20** 6784
[25] Zhu W, Liu X, Liu H, Tong D, Yang J and Peng J 2010 *J. Am. Chem. Soc.* **132** 12619
[26] Kim H, Noh K, Choi C, Khamwannah J, Villwock D and Jin S 2011 *Langmuir* **27** 10191
[27] Yao H, Ma J, Mu Y, Chen Y, Su S, Lv P, Zhang X, Ding D, Fu W and Yang H 2015 *RSC Adv.* **5** 6429
[28] Wassell D T and Embery G 1996 *Biomaterials* **17** 859
[29] Li L, Hu J, Yang W and Alivisatos A P 2001 *Nano Lett.* **1** 349
[30] Takei K, Fang H, Kumar S B, Kapadia R, Gao Q, Madsen M, Kim H S, Liu C H, Chueh Y L, Plis E, Krishna S, Bechtel H A, Guo J and Javey A 2011 *Nano Lett.* **11** 5008
[31] Lee Y L, Chi C F and Liau S Y 2010 *Chem. Mater.* **22** 922
[32] Turaeva N N, Oksengendler B L and Uralov I 2011 *Appl. Phys. Lett.* **98** 243103
[33] Schaller R D and Klimov V I 2004 *Phys. Rev. Lett.* **92** 186601
[34] Pradhan S, Stavrinadis A, Gupta S, Christodoulou S and Konstantatos G 2017 *ACS Energy Lett.* **2** 1444